Journal of Alloys and Compounds 612 (2014) 189–194

Contents lists available at ScienceDirect

Journal of Alloys and Compounds

journal homepage: www.elsevier.com/locate/jalcom

Solid state synthesis and characterization of ferromagnetic nanocomposite Fe–In_2O_3 thin films

V.G. Myagkov [a,b], I.A. Tambasov [a,*], O.A. Bayukov [a], V.S. Zhigalov [a,b], L.E. Bykova [a], Yu.L. Mikhlin [c], M.N. Volochaev [b], G.N. Bondarenko [c]

[a] Kirensky Institute of Physics, Russian Academy of Sciences, Siberian Branch, Krasnoyarsk 660036, Russia
[b] Reshetnev Siberian State Aerospace University, Krasnoyarsk 660014, Russia
[c] Institute of Chemistry and Chemical Technology, Russian Academy of Sciences, Siberian Branch, Krasnoyarsk 660049, Russia

ARTICLE INFO

Article history:
Received 28 January 2014
Received in revised form 23 May 2014
Accepted 23 May 2014
Available online 5 June 2014

Keywords:
Thermite reactions
Reactive films
Ferromagnetic nanocomposite films
Transparent conducting oxides

ABSTRACT

We have successfully synthesized ferromagnetic Fe–In_2O_3 nanocomposite thin films for the first time using the thermite reaction $Fe_2O_3 + In = In_2O_3 + Fe$. The initial In/$Fe_2O_3$ bilayers were obtained by the deposition of In layers on α-Fe_2O_3 films. The reaction occurs in a self-propagating mode in a homogeneous thermal film plane field at heating rates above 20 K/s and at temperatures above initiation temperature $T_{in} \sim 180$ °C. At heating rates lower than 20 K/s the mixing of the In and Fe_2O_3 layers occurs across the whole In/Fe_2O_3 interface and the synthesis of the ferromagnetic α-Fe phase starts above the initiation temperature $T_{in} = 180$ °C. X-ray diffraction, X-ray photoelectron spectroscopy, Mossbauer spectroscopy, transmission electron microscopy and magnetic measurements were used for phase identification and microstructure observation of the synthesized Fe–In_2O_3 samples. The reaction products contain (1 1 0) textured α-Fe nanocrystals with a diameter around 100 nm and surrounded by an In_2O_3 matrix. These results enable new efficient low-temperature methods for synthesizing ferromagnetic nanocomposite films containing ferromagnetic nanoclusters embedded in transparent conducting oxides.

1. Introduction

Magnetic nanocomposites have attracted a great deal of attention, both from a fundamental perspective and for their potential applications based on their acquisition of novel magnetic properties that depend on grain size [1–4] The most common methods for synthesizing magnetic nanocomposites and hybrid materials use wet chemistry; these include sol–gel methods, solvothermal methods, sonochemical synthesis, thermal decomposition, chemical reduction, and radiolysis [1–8]. The obtained systems contain ferromagnetic/ferrimagnetic nanoscale grains that are randomly distributed within the matrix. However, these methods cause negative defects such as pollution, sintering, agglomeration, and a wide variation in the distribution of grains. After wet chemistry, the next most important method of obtaining functional magnetic nanocomposites is the formation of magnetic granular films created from a joint deposition of metal and an insulator [9,10]. The third most important method is related to the formation of ferromagnetic/ferrimagnetic precipitates as a result of spinodal decomposition in dilute magnetic semiconductors (DMS) and dilute magnetic oxides (DMO). The nature of ferromagnetism in DMS and DMO is of great scientific and technological interest [11–19]. The formation of DMS and DMO occurs in doped metals which are embedded into the lattice of the semiconductor or oxide during the formation of the solid solution. The promising candidates for DMO are doped 3d transition metal ions from transparent conducting oxides, such as In_2O_3, ZnO, TiO_2, and SnO_2 [14–17]. However, numerous experiments using different methods have provided contradictory results regarding the ferromagnetic order in identical DMS and DMO samples. The nature of the room magnetism in DMS and DMO is unknown; one explanation is the formation of ferromagnetic precipitates [11–17]. The detection of nanoscale precipitates is an experimentally difficult task. Co nanoclusters have been found in Co-doped ZnO films [18,19]. In recent years, the magnetic properties of Fe-doped In_2O_3 DMO have attracted attention, as Fe ions have high solubility in the In_2O_3 lattice [20].

The magnetic properties of DMO-based Fe-doped In_2O_3 strongly depend on its preparation method. Some studies show that they are paramagnetic [21]; however, other studies show ferromagnetic properties [22–24] or low magnetization [25–30]. To date, there

* Corresponding author.
E-mail address: tambasov_igor@mail.ru (I.A. Tambasov).

http://dx.doi.org/10.1016/j.jallcom.2014.05.176
0925-8388/

has been no evidence of ferromagnetic nanocluster formation in Fe-doped In_2O_3. Also, there are no methods for obtaining Fe–In_2O_3 nanocomposites, which represent an important functional class of magnetic nanocomposites that contain components of transition 3d metals or magnetic compounds on their basis and transparent conducting oxides.

The present work uses the thermite reaction

$$Fe_2O_3 + In = In_2O_3 + Fe. \quad (1)$$

We demonstrate a new method for synthesizing Fe–In_2O_3 nanocomposite films containing ferromagnetic α-Fe clusters with a diameter of 100 nm or less and surrounded by a In_2O_3 matrix. Reaction (1) is analogous to the classical thermite reaction $Fe_2O_3 + Al = Al_2O_3 + Fe$, which has been known for more than 100 years and was previously used in the connection of railway lines [31–33]. Thermite mixtures belong to a wide class of energetic materials that contain a metal fuel (for example, Al, Mg, and B) and an oxidizer (Fe_2O_3, MoO_3, CuO, Bi_2O_3, and WO_3). These mixtures react with a release of large quantities of heat and may have a self-propagating high-temperature synthesis mode. Typical energetic mixtures containing micron-sized particles have a combustion wave velocity on the order of 0.01–20 m/s [31–33]. In nanocomposite thermites (also termed nanostructured metastable intermolecular composites or nanothermites), for which the size of the particles is reduced to the nanoscale, the combustion wave velocity is increased by two to three orders of magnitude, reaching 1000 m/s [34]. Nanostructured metastable intermolecular composites in the form of multilayer free-standing foils, such as Ni/Al, NiTi, Ni/Zr, Co/Al, Al/Ti, Nb/Si and CuO/Al have reaction wave velocities in the range of 0.5–15 m/s [35–42].

It is well known that in thin film solid state reactions the atom mixing and the formation of compounds start at relatively low temperatures. The unique feature of thin film solid state reactions is the formation of only one phase (the first phase) at the interface of the thin film bilayers. Further increases in temperature lead to the formation of a phase sequence. The first phase, characterized by the initiation temperature T_{in}, is experimentally observed in thin film bilayers only above T_{in}. To date, the formation of the first phase, the phase sequence and the initiation temperatures of the phases have not been explained, although several models have been proposed [43–45]. For the most reactive bilayers connected to the substrate, the solid-state reaction between the layers starts in a self-propagating mode only above the initiation temperature T_{ir} and with a heating rate exceeding >20 K/s. For the Ni/Al [46] and Al/Fe_2O_3 [47] bilayers, the initiation temperatures are T_{in}(Ni/Al) ~ 220 °C and T_{in}(Al/Fe_2O_3) ~ 530 °C, respectively. It is important to note that at a heating rate of ~ 20 K/s, the self-propagation reaction velocities in the Ni/Al and Al/Fe_2O_3 bilayers deposited on glass substrates are more than 2–3 orders of magnitude less than those for free-standing foils. The velocity is about 0.5 cm/s at temperatures somewhat exceeding T_{in}, and it greatly increases with the increase of the substrate temperature T_S. This implies that the substrate is a heat sink that greatly reduces the reaction front velocity. Although self-propagating reactions in nanofilms have been intensively studied, their regularities and mechanisms are not sufficiently understood [35].

2. Experimental section

2.1. Synthesis

Starting films were obtained by the thermal deposition of Fe layers at a temperature of 250 °C onto NaCl(001) and chemically pure glass substrates having a thickness of 0.18 mm in a vacuum at a residual pressure of 10^{-6} Torr. In the preliminary work, the substrates were degassed at 350 °C for 1 h. The α-Fe_2O_3 films were obtained by oxidation in an air environment of the starting Fe films at a temperature of 350 °C. The top In layer was deposited at room temperature to prevent a reaction between In and Fe_2O_3 during deposition. In these experiments, we used In/Fe_2O_3 bilayers with an approximate 1Fe:1In stoichiometry.

Three methods were used to initiate the exothermic reaction in the In/Fe_2O_3 bilayers. All synthesized Fe–In_2O_3 samples were obtained at pressure of 10^{-6} Torr.

In the first method, the initial In/Fe_2O_3 bilayers were placed on a flat tungsten heater, creating a homogeneous film plane thermal field. In previous studies we have shown that the first method allows two modes of reaction for some reactive bilayers connected with the substrate [46–48]. Increasing the temperature above the initiation temperature T_{in} and the heating rates above 20 K/s {explosive heating} causes the reaction to occur in an autowave regime. In this case, the nucleus of the reaction products began materializing on the film surface at the point (usually in the film center) where the temperature exceeds the initiation temperature. The nucleus radius grew until it was spread along the entire film surface. However, at a heating rate below 20 K/s (slow heating) and the same experimental conditions, the reaction goes to completion transversely across the full sample surface. The thermal mechanism of the autowave regime is discussed in detail elsewhere [46–48].

The second method was used for creating the directional movement of the reaction front. For this purpose, the edge of the initial In/Fe_2O_3 film was heated to create a temperature gradient along the film surface. Increasing the temperature of the film edge above the initiation temperature T_{in} ~ 180 °C caused the reaction product nucleus to arise and the reaction front to move to the cold part of the sample.

In the third method, the initial In/Fe_2O_3 bilayers were annealed at temperatures between 50–400 °C at 50 °C intervals. To find the initiation temperature T_{in} ~ 180 °C, the samples were annealed at temperatures between 160–200 °C in 10 °C intervals. The samples were held at each temperature for 2 h.

An important point is that the initiation temperature T_{in} ~ 180 °C and the synthesized phases are independent from the initiation methods. Based on ~~a~~ resistivity and magnetic studies there is experimental evidence that the post-reaction processes completely finished after annealing at 300 °C for 2 h. In this work results are given for synthesized Fe–In_2O_3 samples obtained by the third method of annealing at 300 °C for 2 h. Films on NaCl(001) with thicknesses Fe ~ 20 nm and In ~ 40 nm were prepared for the electron microscopy studies. In the rest of the experiments we used films on glass substrates with a total thickness of 50–400 nm and only experimental results for films with thicknesses Fe ~ 100 nm, In ~ 200 nm are presented here.

2.2. Characterization

The morphology and chemical composition of the films was investigated by transmission electron microscopy (TEM) using a JEOL JEM-2200FS system. The phases formed during synthesis process were identified using a DRON-4007 X-ray diffractometer (Cu Kα radiation). An energy-dispersive X-ray (EDX) spectroscopy line scan was performed in scanning TEM mode with an electron probe of diameter ~2 nm. The chemical states were characterized by X-ray photoelectron spectroscopy (XPS). XPS spectra were obtained on a SPECS photoelectron spectrometer (Germany) with the use of an X-ray tube for exciting the Mg Kα radiation spectra (1253.6 eV). The relative concentrations of elements were determined by the plain X-ray spectra recorded at a transmission energy of 20 eV on a PHOIBOS 150 MCD9 hemispherical energy analyzer using empirical sensitivity coefficients. Mossbauer measurements were performed on a MS–1104Em spectrometer with a Co^{57}(Cr) source. The saturation magnetization M_S was measured on an MPMS-XL SQUID magnetometer (Quantum Design) on in-plane magnetic fields. The resistance was measured by a standard four-probe method.

3. Results and discussion

The starting α-Fe films had a saturation magnetization (M_S^0 = 217 emu/g) coinciding with the saturation magnetization of bulk samples. Oxidation in air led to the formation of an α-Fe_2O_3 phase and a sharp reduction of magnetization up to 2 emu/g. Since the magnetization of the α-Fe_2O_3 phase at room temperature is approximately 0.127 emu/g [49]. It follows that the oxidation products contain a small amount of magnetic oxides, such as γ-Fe_2O_3 and Fe_3O_4, in addition to the principal α-Fe_2O_3 phase. To avoid reactions between In and Fe_2O_3, the initial In/Fe_2O_3 bilayers were obtained from the deposition of the In layer on Fe_2O_3 film at room temperature. The magnetization of the samples did not change after the deposition of the In layer. The diffraction patterns of the initial In/Fe_2O_3 bilayers contained reflections from the polycrystalline In and α-Fe_2O_3 phases (Fig. 1a). These data provide clear evidence that the initial samples are In/Fe_2O_3 bilayers.

Using the first method, the initial In/Fe_2O_3 bilayers were placed on a flat tungsten heater and heated at a rate above 20 K/s to a

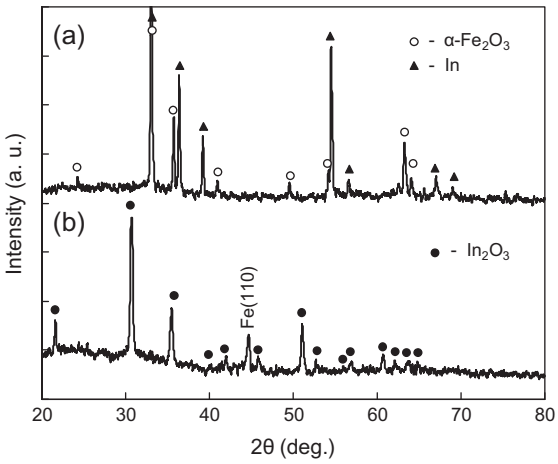

Fig. 1. (a) Typical XRD pattern of the initial In/Fe_2O_3 bilayers and (b) the synthesized $Fe–In_2O_3$ nanocomposites at 300 °C for 2 h.

temperature of 400 °C. Our studies showed that the high heating rate above 20 K/s is a necessary condition for the initiation of reactive waves in bilayers connected with the substrate [46–48]. A front reaction occurs at temperatures above the initiation temperature $T_{in} \sim 180$ °C and has a propagation velocity ~0.5 cm/s. The appearance of the nucleus and the front propagation were observed visually. Main features, such as the occurrence of the nucleus and a front velocity of approximately 0.5 cm/s, are the same for many reactive bilayers connected with the substrate [46–48]. These characteristics are strongly distinguished from self-propagation reactions in multilayer foils (without a substrate), which are initiated by local heating and have large reaction front velocities (above 15 m/s) [33–41].

In the temperature gradient field (second method) the reaction front stops at a place where the temperature equals the temperature of initiation $T_{in} \sim 180$ °C. Since the melting temperature of In ($T_m = 156$ °C) is less than the initiation temperature, the melting front of In precedes the reaction front (Fig. 2).

The third method has been used to find the reduced iron amount vs. the annealing temperature and the initiation temperature. Annealing in 10 °C increments around 180 °C was carried out to obtain the true value of the initiation temperature.

Up to 180 °C the saturation magnetization M_S in the In/Fe_2O_3 bilayers did not change, which indicates there was no mixing or reaction between the In and Fe_2O_3 layers. After annealing above 200 °C, the saturation magnetization M_S greatly increased and

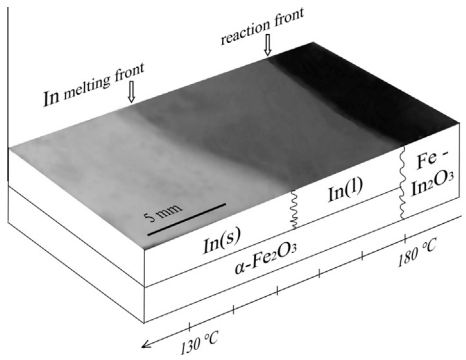

Fig. 2. Photograph of surface and reaction front propagation in In/Fe_2O_3 bilayers in a 40 °K/cm gradient temperature field. The reaction front stops at the location of the film, which has an initiation temperature $T_{ig} = 180$ °C. The reaction front precedes the melting layer front of In.

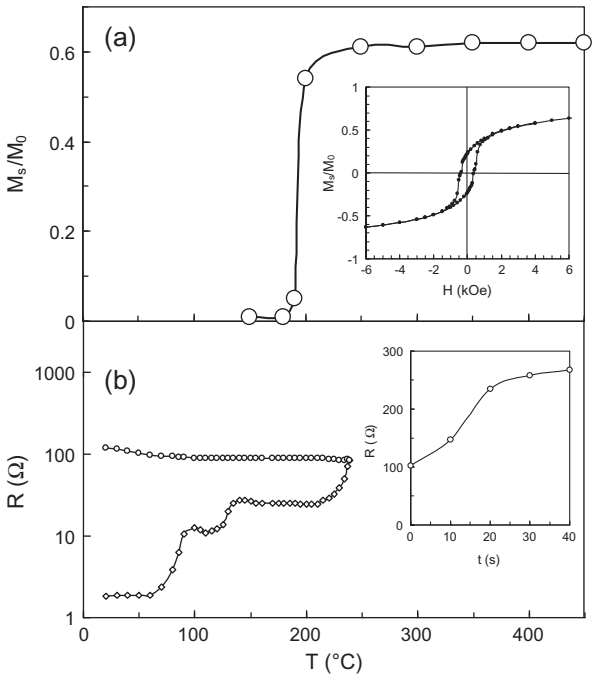

Fig. 3. (a) Relative magnetization M_S/M_0 as a function of annealing temperature for In/Fe_2O_3 bilayers. The inset shows the hysteresis loop of the synthesized $In–Fe_2O_3$ nanocomposite at room temperature and (b) resistivity as a function of temperature measurement heated at 2 °K/min to 250 °C for In/Fe_2O_3 bilayers. The inset shows resistivity vs. annealing time at 250 °C.

reached a maximum of $M_S \sim 0.65\ M_S^0$ above 300 °C (Fig. 3a). The beginning of the magnetization increase at 180 °C and its strong growth at 200 °C are associated with the mixing of the In and Fe_2O_3 layers and the synthesis of the ferromagnetic α-Fe phase in the reaction product layer. Within experimental accuracy, the initiation temperature $T_{in} = 180$ °C does not depend on the substrate type and the initiation method of the Reaction (1). The formation of the α-Fe phase is consistent with diffraction data showing a reflection from (1 1 0) Fe and polycrystalline In_2O_3 phases (Fig. 1b). There is no trace belonging to other Fe–O and Fe–In–O compounds.

The inset of Fig. 3a presents a typical in-plane hysteresis loop of a synthesized $Fe–In_2O_3$ film at room temperature, which is close to the shape of the hysteresis loop ensemble of single-domain particles described by Stoner–Wohlfartht theory [50]. This implies that the synthesized $Fe–In_2O_3$ film contains α-Fe nanoparticles separated by In_2O_3 interlayers.

Fig. 3b shows resistivity vs. temperature for In/Fe_2O_3 bilayers that are heated at 2 K/min to 250 °C (the first method, slow heating) and cooled to room temperature. The first phase transformation in the initial In/Fe_2O_3 bilayers creates a feature in the $R(T_S)$ plot around 100 °C. We propose that this feature is associated with pre-melting in the indium layer. The increase in temperature above 180 °C leads to a rapid increase in resistivity, which is undoubtedly connected with the initiation and development of Reaction (1). Resistivity above $T_{in} = 180$ °C depends on the time of annealing, as shown in the inset of Fig. 3b. These changes are connected with the afterburning and structural relaxation in the In/Fe_2O_3 bilayers, which at 250 °C are fully completed after 2 h.

After annealing above 250 °C, the maximum magnetization M_S of the synthesized $Fe–In_2O_3$ films is about 0.65 M_S^0 of the saturation magnetization ($M_S^0 = 217$ emu/g) of the initial Fe film (Fig. 3a). It follows from this and Reaction (1) that no more than 65% of the volume of the initial α-Fe film is reduced In. Further structural and morphological characterization of the $Fe–In_2O_3$ films were

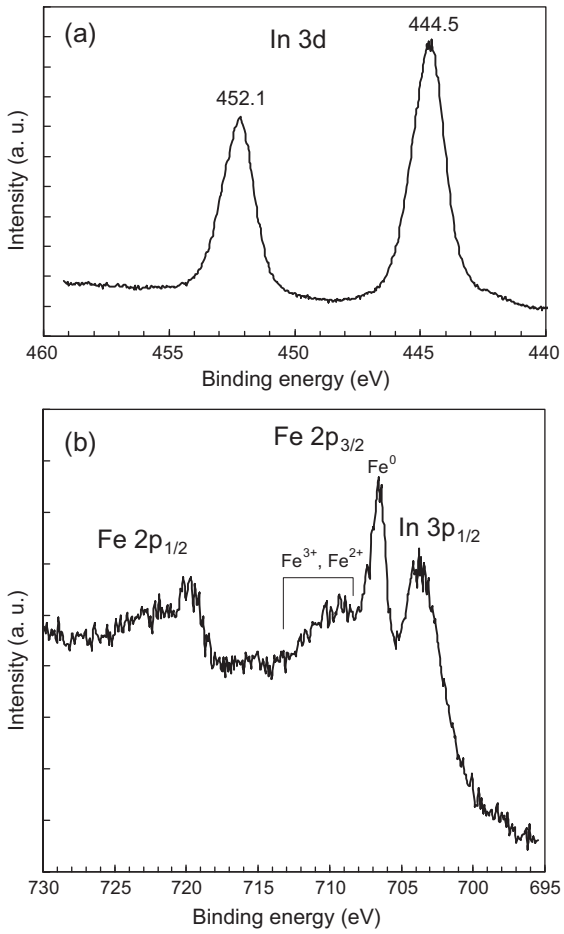

Fig. 4. (a) XPS of In 3d peaks and (b) Fe 2p peaks for the synthesized In–Fe_2O_3 nanocomposite after annealing at 300 °C for 2 h.

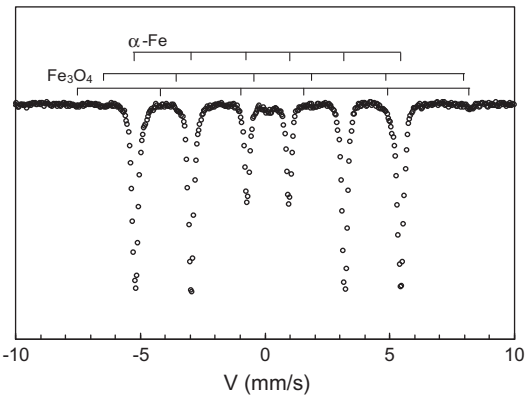

Fig. 5. Room temperature Mossbauer spectra of the synthesized Fe–In_2O_3 nanocomposite after annealing at 300 °C for 2 h.

obtained using X-ray photoelectron spectroscopy (XPS), Mössbauer spectroscopy, and transmission electron microscopy (TEM).

Fig. 4 shows the typical In 3d and Fe 2p photoelectron spectra of the sintered Fe–In_2O_3 film, after etching with Ar^+ ions to remove the surface oxidized layer. The position of the In $3d_{5/2}$ peak at a binding energy of 444.5 eV is in close agreement with the values reported for In_2O_3. The energy difference between the In $3d_{5/2}$ and $3d_{3/2}$ peaks is 7.6 eV, which confirms the formation of the In_2O_3 phase (Fig. 4a) [51]. A narrow Fe $2p_{3/2}$ peak at 707.0 eV in the iron spectrum (partially overlapping the In $3p_{1/2}$ band) corresponds to metallic Fe. The broad bands at higher binding energies are attributed to a series of multiplet peaks, from Fe^{3+} in γ-Fe_2O_3, and α-Fe_2O_3 and probably Fe^{2+} in Fe_3O_4 (Fig. 4b) [52]. The relative intensity of the features suggests that up to 35% of the iron atoms occur in the oxide phases. This estimate is consistent with the value obtained from magnetic measurements (see Fig. 3a).

The Mössbauer spectrum of synthesized Fe–In_2O_3 films was recorded at room temperature as being the gamma rays perpendicular to the substrate plane (Fig. 5). The parameters of this spectrum are given in Table 1. The main component (98%) of the Fe–In_2O_3 film spectra is α-Fe. The ratio of the sextet line amplitudes testifies that the direction of a hyperfine field, or the magnetic moment of Fe atoms, makes a 60° angle with the gamma ray direction. It is in agreement with the (1 1 0) textured growth of Fe on glass substrates, which was detected by X-ray diffraction. The second component (2%) contains iron of mixed-valence $Fe^{2.5+}$, which indicates that the sample contains magnetite. The difference in the estimates of the Fe_3O_4 fraction, obtained from Mossbauer data and magnetic and XPS measurements, can be linked with the difference in the probability of the Mössbauer effect for these phases [53] .The third component is the small singlet in the center of the spectrum with zero chemical shift, which can be associated to a small amount (<1%) of paramagnetic γ-Fe. None of the Mossbauer data indicates the presence of other iron oxides or phases of the Fe–In–O system.

Fig. 6a shows a typical bright field TEM image of the synthesized Fe–In_2O_3 film and nanoparticles with an effective average size about 100 nm that are uniformly distributed over the surface. The area between these nanoparticles is filled with nanoparticles that are 20–40 nm. The average atomic number for the In_2O_3 phase is lower than the atomic number of α-Fe and the In_2O_3 region appears brighter than the α-Fe region. From the TEM image (Fig. 6a) it is clearly seen that the α-Fe nanoparticles are clustered (dark region) and are separated by an In_2O_3 matrix (bright region). Fig. 6b shows the energy-dispersive X-ray (EDX) line scan across an Fe–In_2O_3 nanoparticle. The line profiles of Fe, In, and O in Fig. 6b indicate that iron is located near the center and is enveloped by an In_2O_3 shell, clearly confirming the formation of an Fe/In_2O_3 core/shell-like morphology.

We noticed that the initiation temperature T_{in} = 180 °C of Reaction (1) coincides with the initiation temperature of the self-sustaining oxidation of In [54]. Therefore, the synthesis of In_2O_3 does not depend on whether the In atoms are in the In/Fe_2O_3 bilayers or in the atmosphere. This suggests a possible mechanism for the formation of the nanocomposite structure of the Fe–In_2O_3 films. Strong chemical interactions between the In and O atoms occur above 180 °C, which break the chemical bonds in the original In and Fe_2O_3 lattices and cause the migration of In atoms in the Fe_2O_3 layer and oxygen atoms in the Fe_2O_3 grains. The migration of oxygen atoms in the Fe_2O_3 grain boundaries induces a restructuring of the grain and the formation of α-Fe nanoclusters. Since In is immiscible with Fe, the Indium atoms moving along the grain boundary react with the oxygen located on the grain borders. A result is the formation of Fe–In_2O_3 core/shell-like nanostructures.

The negative heats of formation of Al_2O_3 (ΔH_f = −1676 kJ/ mol) and In_2O_3 (ΔH_f = −923.5 kJ/mol), which are less than the negative heat of formation of Fe_2O_3 (ΔH_f = −824.2 kJ/ mol), are the driving forces behind the thermite Fe_2O_3 + Al and Fe_2O_3 + In reactions, respectively. Although the reaction enthalpy of Fe_2O_3 + Al significantly exceeds the reaction enthalpy of Fe_2O_3 + In, both reactions in the In/Fe_2O_3 and Al/Fe_2O_3 bilayers deposited on substrates have similar kinetic characteristics. Thus, both reactions occur with a self-propagating mode at heating rates above >20 K/s, and the reaction front velocities strongly increase with increasing heating rate. At heating rates <20 K/s, both reactions proceed in a reaction diffusion mode, but this does not change their initiation temperature. A minor difference is that the ignition temperatures

Table 1
Mössbauer parameters for synthesized Fe–In_2O_3 nanocomposites.

IS, mm/s ± 0.02	H, kOe ± 3	QS, mm/s ± 0.02	W, mm/s ± 0.02	Θ, grad ± 5	A ± 0.03	Phase
−0.02	330	0	0.39	61	0.98	α-Fe
0.26	494	0	0.15	84	0.004	Fe_3O_4 (Fe^{3+})
0.68	455	0.24	0.21	84	0.014	Fe_3O_4 ($Fe^{2.5+}$)

Here *IS* is the isomer chemical shift relative to α-Fe, ±0.02 mm/s; *H* is the hyperfine magnetic field on Fe nuclei, ±5 kOe; *QS* is the quadrupole shift or splitting, ±0.03 mm/s; *W* is the linewidth of absorption, ±0.03 mm/s; *S* is the relative spectral area, ± 0.05.

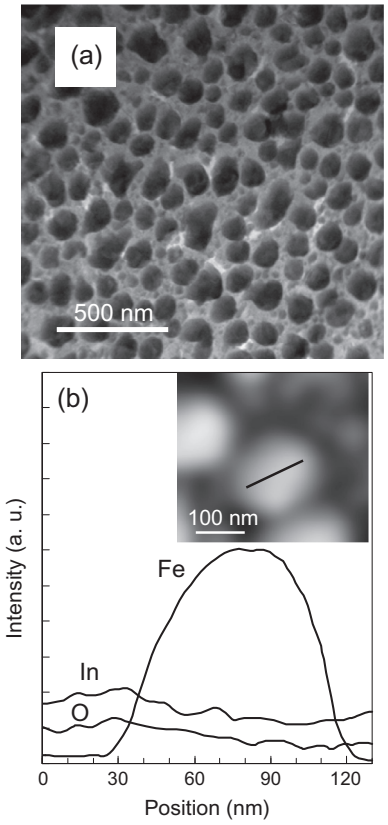

Fig. 6. TEM image of (a) Fe nanoparticles embedded in the In_2O_3 matrix and (b) the TEM image and EDS profiles of concentrations of Fe, In, and O along the line across the particle in a Fe–In_2O_3 nanocomposite.

were $T_{in}(In/Fe_2O_3) = 180$ °C above the In melting point $T_m(In) = 156$ °C, and $T_{ig}(Al/Fe_2O_3) = 530$ °C below the Al melting point $T_mAl = 660$ °C.

Above, we showed that about 35% of the iron is in an oxide form in the reaction products. The magnetization of the synthesized Fe–In_2O_3 sample has a step increase at a temperature around 120 K, which is associated with the well-known Verwey transition and is the signature of the Fe_3O_4 phase. As the temperature decreases below the Verwey transition, the magnetization of the Fe_3O_4 phase is reduced by 25% [55]. Taking magnetization values of the Fe and Fe_3O_4 phases to be equal to the values of the massive samples, we estimated that the share of the Fe_3O_4 phase in the synthesized Fe–In_2O_3 samples is about 20–25%. From this it is necessary to assume that ~15–10% of the unreacted Fe_2O_3 remained in the synthesized Fe–In_2O_3 sample. Secondary phases, including Fe_3O_4, can also be formed in Al + Fe_2O_3 thermite reactions, both as micron-sized powders [32,33] and as nanothermite systems [56].

Since Reaction (1) concludes after annealing at 300 °C, the synthesized Fe–In_2O_3 sample has a good temperature stability and samples at room temperature do not change magnetic properties for 1 year. The heating rate and the choice of subsequent annealing conditions are controlling parameters that determine the formation of nanostructures, which in turn determine the physicochemical properties of nanocomposite Fe–In_2O_3 thin films.

In summary, we have demonstrated a new way to synthesize ferromagnetic Fe–In_2O_3 nanocomposite thin films. The thermite reaction (1), using In and Fe_2O_3 films as a fuel and an oxidizer in In/Fe_2O_3 bilayers, starts above the initiation temperature $T_{in} = 180$ °C with the predominant formation of Fe and In_2O_3 phases. At heating rates above 20 K/s, the reaction occurs in a self-propagating mode in which the In melting front precedes the reaction front. The reaction products contains (110) texturated α-Fe nanocrystals enveloped by a In_2O_3 shell. Our finding predicts an entire family of solid state thin film reactions between oxides of transition 3d metals and metals such as Zn, Sn, Cd, or Ti. These reactions synthesize ferromagnetic nanocomposites containing ferromagnetic nanoclusters embedded in ZnO, SnO_2, CdO, or TiO_2 matrices.

Acknowledgments

The authors also wish to thanks Dr. A.G. Chirkov for the TEM observations and Dr. D.A. Velikanov for assisting with the magnetic measurements of the samples.

References

[1] S. Behrens, Preparation of functional magnetic nanocomposites and hybrid materials: recent progress and future directions, Nanoscale 3 (2011) 877–892.
[2] R. Ferrando, J. Jellinek, R.L. Johnston, Nanoalloys: from theory to applications of alloy clusters and nanoparticles, Chem. Rev. 108 (2008) 845–910.
[3] K.C.-F. Leung, S. Xuan, X. Zhu, D. Wang, C.-P. Chak, S.-F. Lee, W.K.-W. Ho, B.C.-T. Chung, Gold and iron oxide hybrid nanocomposite materials, Chem. Soc. Rev. 41 (2012) 1911–1928.
[4] S. Wei, Q. Wang, J. Zhu, L. Sun, H. Line, Z. Guo, Multifunctional composite core-shell nanoparticles, Nanoscale 3 (2011) 4474–4502.
[5] R.G. Chaudhuri, S. Paria, Core/shell nanoparticles: classes, properties, synthesis mechanisms, characterization, and applications, Chem. Rev. 112 (2012) 2373–2433.
[6] L. Carbone, P.D. Cozzoli, Colloidal heterostructured nanocrystals: synthesis and growth mechanisms, Nano Today 5 (2010) 449–493.
[7] P. Reiss, M. Protière, L. Li, Core/shell semiconductor nanocrystals, Small 5 (2009) 154–168.
[8] S. Mann, Self-assembly and transformation of hybrid nano-objects and nanostructures under equilibrium and non-equilibrium conditions, Nat. Mater. 8 (2009) 781–792.
[9] K. Sato, M. Mizuguchi, R. Tang, J.-G. Kang, M. Ishimaru, K. Takanashi, T.J. Konno, Direct imaging of atomic clusters in an amorphous matrix: a Co–C granular thin film, Appl. Phys. Lett. 101 (2012) 191902-1–191902-3.
[10] K. Yakushiji, S. Mitani, F. Ernult, K. Takanashi, H. Fujimori, Spin-dependent tunneling and Coulomb blockade in ferromagnetic nanoparticles, Phys. Rep. 451 (2007) 1–35.
[11] M. Jamet, A. Barski, T. Devillers, V. Poydenot, R. Dujardin, P. Bayle-Guillemaud, J. Rothman, E. Bellet-Amalric, A. Marty, J. Cibert, R. Mattana, S. Tatarenko, High-Curie-temperature ferromagnetism in self-organized $Ge_{1-x}Mn_x$ nanocolumns, Nat. Mater. 5 (2006) 653–659.
[12] T. Dietl, A ten-year perspective on dilute magnetic semiconductors and oxides, Nat. Mater. 9 (2010) 965–974.
[13] A. Bonanni, T. Dietl, A story of high-temperature ferromagnetism in semiconductors, Chem. Soc. Rev. 39 (2010) 528–539.
[14] J.M.D. Coey, Dilute magnetic oxides, Curr. Opn. Solid State Mater. 10 (2006) 83–92.
[15] S. Zhou, K. Potzger, J. von Borany, R. Grötzschel, W. Skorupa, M. Helm, J. Fassbender, Crystallographically oriented Co and Ni nanocrystals inside ZnO formed by ion implantation and postannealing, Phys. Rev. B 77 (2008) 035209-1–035209-12.

[16] S.A. Chambers, Ferromagnetism in doped thin-film oxide and nitride semiconductors and dielectrics, Surf. Sci. Rep. 61 (2006) 345–381.
[17] S.B. Ogale, Dilute doping, defects, and ferromagnetism in metal oxide systems, Adv. Mater. 22 (2010) 3125–3155.
[18] J.H. Park, M.G. Kim, H.M. Jang, S. Ryu, Y.M. Kim, Co-metal clustering as the origin of ferromagnetism in Co-doped ZnO thin films, Appl. Phys. Lett. 84 (2004) 1338–1340.
[19] M. Godlewski, E. Guziewicz, M.I. Łukasiewicz, I.A. Kowalik, M. Sawicki, B.S. Witkowski, R. Jakieła, W. Lisowski, J.W. Sobczak, M. Krawczyk, Role of interface in ferromagnetism of (Zn, Co)O films, Phys. State Solidi (b) 248 (2011) 1596–1600.
[20] J. He, S. Xu, Y.K. Yoo, Q. Xue, H.-C. Lee, S. Cheng, X.-D. Xiang, G.F. Dionne, I. Takeuchi, Room temperature ferromagnetic n-type semiconductor inÂ $(In_{1-x}Fe_x)_2O_{3-\sigma}$, Appl. Phys. Lett. 86 (2005) 052503-1–052503-3.
[21] D. Bérardan, E. Guilmeau, D. Pelloquin, Intrinsic magnetic properties of In_2O_3 and transition metal-doped-In_2O_3, J. Magn. Magn. Mater. 320 (2008) 983–989.
[22] O.D. Jayakumar, I.K. Gopalakrishnan, S.K. Kulshreshtha, A. Gupta, K.V. Rao, D.V. Louzguine-Luzgin, A. Inoue, P.-A. Glans, J.-H. Guo, K. Samanta, M.K. Singh, R.S. Katiyar, Structural and magnetic properties of $(In_{1-x}Fe_x)_2O_3$ $(0.0 < x < 0.25)$ system: prepared by gel combustion method, Appl. Phys. Lett. 91 (2007) 052504-1–052504-3.
[23] P.F. Xing, Y.X. Chen, S.-S. Yan, G.L. Liu, L.M. Mei, K. Wang, X.D. Han, Z. Zhang, High temperature ferromagnetism and perpendicular magnetic anisotropy in Fe-doped In_2O_3 films, Appl. Phys. Lett. 92 (2008) 022513-1–022513-3.
[24] Y.K. Yoo, Q, Xue, H.-C. Lee, S. Cheng, X.-D. Xiang, G.F. Dionne, S. Xu, J. He, Y.S. Chu, S.D. Preite, S.E. Lofland, I. Takeuchi, Bulk synthesis and high-temperature ferromagnetism of $(In_{1-x}Fe_x)_2O_{3-\sigma}$ with Cu co-doping, Appl. Phys. Lett. 86 (2005) 042506-1–042506-3.
[25] Y.K. Yoo, Q. Xue, H.-C. Lee, S. Cheng, X.-D. Xiang, G.F. Dionne, S. Xu, J. He, Y.S. Chu, S.D. Preite, S.E. Lofland, I. Takeuchi, Bulk synthesis and high-temperature ferromagnetism of $(In_{1-x}Fe_x)_2O_{3-\sigma}$ with Cu co-doping, Appl. Phys. Lett. 86 (2005) 042506-1–042506-3.
[26] F.-X. Jiang, X.-H. Xu, J. Zhang, X.-C. Fan, H.-S. Wu, M. Alshammari, Q. Feng, H.J. Blythe, D.S. Score, K. Addison, M. Al-Qahtani, G.A. Gehring, Room temperature ferromagnetism in metallic and insulating $(In_{1-x}Fe_x)_2O_3$ thin films, J. Appl. Phys. 109 (2011) 053907-1–053907-7.
[27] S. Yan, S. Ge, W. Qiao, Y. Zuo, F. Xu, L. Xi, Control of ferromagnetism in Fe-doped In_2O_3 by carbothermal annealing, J. Magn. Magn. Mater. 323 (2011) 264–267.
[28] H. Kim, M. Osofsky, M.M. Miller, S.B. Qadri, R.C.Y. Auyeung, A. Piqué, Room temperature ferromagnetism in transparent Fe-doped In_2O_3 films, Appl. Phys. Lett. 100 (2012) 032404-1–032404-3.
[29] S. Yan, K. Liu, G. Lv, Z. Fan, Fluorine doping inducing high temperature ferromagnetism in $(In_{1-x}Fe_x)_2O_3$, J. Alloys Comp. 551 (2013) 40–43.
[30] E. Pellicer, M. Cabo, E. Rossinyol, P. Solsona, S. Suriñach, M.D. Baró, J. Sort, Nanocasting of mesoporous In–TM (TM = Co, Fe, Mn) oxides: towards 3D diluted-oxide magnetic semiconductor architectures, Adv. Funct. Mater. 23 (2013) 900–911.
[31] L.L. Wang, Z.A. Munir, Y.M. Maximov, Thermite reactions: their utilization in the synthesis and processing of materials, J. Mater. Sci. 28 (1993) 3693–3708.
[32] Y. Yang, D.-r. Yan, Y.-c. Dong, X.-g. Chen, L. Wang, Z.-h. Chu, J.-x. Zhang, J.-n. He, Influence of oxides addition on the reaction of Fe_2O_3–Al composite powders in plasma flame, J. Alloys Comp. 579 (2013) 1–6.
[33] A. Babakhani, E. Zahabi, H.Y. Mehrabani, Fabrication of Fe/Al_2O_3 composite foam via combination of combustion synthesis and spark plasma sintering techniques, J. Alloys Comp. 514 (2012) 20–24.
[34] A.S. Rogachev, A.S. Mukasyan, Combustion of heterogeneous nanostructural systems (review), Combus. Explos. Shock Waves 46 (2010) 243–266.
[35] A.S. Rogachev, Exothermic reaction waves in multilayer films, Russ. Chem. Rev. 77 (2008) 21–37.
[36] R. Knepper, M.R. Snyder, G. Fritz, K. Fisher, O.M. Knio, T.P. Weihs, Effect of varying bilayer spacing distribution on reaction heat and velocity in reactive Al/Ni multilayers, J. Appl. Phys. 105 (2009) 083504-1–083504-9.
[37] J.S. Kim, T. LaGrange, B.W. Reed, M.L. Taheri, M.R. Armstrong, W.E. King, N.D. Browning, G.H. Campbell, Imaging of transient structures using nanosecond in situ TEM, Science 321 (2008) 1472–1475.
[38] D.P. Adams, M.A. Rodriguez, J.P. McDonald, M.M. Bai, E. Jones, Jr., L. Brewer, J.J. Moore, Reacotive Ni/Ti nanolaminates, J. Appl. Phys. 106 (2009) 093505-1–093505-8.
[39] S.C. Barron, R. Knepper, N. Walker, T.P. Weihs, Characterization of self-propagating formation reactions in Ni/Zr multilayered foils using reaction heats, velocities, and temperature-time profiles, J. Appl. Phys. 109 (2011) 013519.
[40] D.P. Adams, V.C. Hodges, M.M. Bai, E. Jones Jr., M.A. Rodriguez, T. Buchheit, J.J. Moore, Exothermic reactions in Co/Al nanolaminates, J. Appl. Phys. 104 (2008) 043502-1–043502-7.
[41] J.-C. Gachon, A.S. Rogachev, H.E. Grigoryan, E.V. Illarionova, J.-J. Kuntz, D.Yu. Kovalev, A.N. Nosyrev, N.V. Sachkova, P.A. Tsygankov, On the mechanism of heterogeneous reaction and phase formation in Ti/Al multilayer nanofilms, Acta Mater. 53 (2005) 1225–1231.
[42] K.J. Blobaum, M.E. Reiss, J.M. Plitzko Lawrence, T.P. Weihs, Deposition and characterization of a self-propagating CuO_x/Al thermite reaction in a multilayer foil geometry, J. Appl. Phys. 94 (2003) 2915–2922.
[43] E.G. Colgan, A review of thin-film aluminide formation, Mater. Sci. Rep. 5 (1990) 1–44.
[44] R. Pretorius, C.C. Theron, A. Vantomme, J.W. Mayer, Compound phase formation in thin film structures, Crit. Rev. Solid State Mater. Sci. 24 (1999) 1–62.
[45] T. Laurila, J. Molarius, Reactive phase formation in thin film metal/metal and metal/silicon diffusion couples, Crit. Rev. Solid. State Mater. Sci. 28 (2003) 185–230.
[46] V.G. Myagkov, L.E. Bykova, S.M. Zharkov, G.V. Bondarenko, Fofmation of NiAl shape memory alloy thin films by solid-state reaction, Solid State Phenomena 138 (2008) 377–384.
[47] V.G. Miagkov, K.P. Polyakova, G.N. Bondarenko, V.V. Polyakov, Granular Fe–Al_2O_3 films prepared by self-propagating high temperature synthesis, J. Magn. Magn. Mater. 258–259 (2003) 358–360.
[48] V.G. Myagkov, L.A. Li, L.E. Bykova, I.A. Turpanov, P.D. Kim, G.V. Bondarenko, G.N. Bondarenko, Self-propagating high-temperature synthesis in Pt/Co/MgO(001) epitaxial thin films, Phys. Solid State 42 (2000) 968–972.
[49] R. Skomski, J.M.D. Coey, Permanent Magnetism, Institute of Physics, Bristol, 1999.
[50] E.C. Stoner, E.P. Wohlfarth, A mechanism of magnetic hysteresis in heterogeneous alloys, Philos. Trans. R Soc. London, Ser. A 240 (1948) 599–642.
[51] R. Henríquez, E. Muñoz, E.A. Dalchiele, R.E. Marotti, F. Martín, D. Leinen, J.R. Ramos-Barrado, H. Gómez, Electrodeposition of In_2O_3 thin films from a dimethylsulfoxide based electrolytic solution, Phys. State Solidi (a) 210 (2013) 297–305.
[52] M.C. Biesinger, B.P. Payne, A.P. Grosvenor, L.W.M. Lau, A.R. Gerson, R.St.C. Smart, Resolving surface chemical states in XPS analysis of first row transition metals, oxides and hydroxides: Cr, Mn, Fe, Co and Ni, Appl. Surf. Sci. 257 (2011) 2717–2730.
[53] V.I. Goldanskii, R.H. Herber (Eds.), Chemical Applications of Mossbauer Spectroscopy, Academic press, New York and London, 1968.
[54] I.A. Tambasov, V.G. Myagkov, A.A. Ivanenko, I.V. Nemtsev, L.E. Bykova, G.N. Bondarenko, Yu.L. Mikhlin, I.A. Maksimov, V.V. Ivanov, S.V. Balashov, D.S. Karpenko, Structural and optical properties of thin In_2O_3 films produced by autowave oxidation, Semiconductor 47 (2013) 569–573.
[55] S.B. Ogale, K. Ghosh, R.P. Sharma, R.L. Greene, R. Ramesh, T. Venkatesan, Magnetotransport anisotropy effects in epitaxial magnetite (Fe_3O_4) thin films, Phys. Rev. B 57 (1998) 7823–7828.
[56] J.L. Cheng, H.H. Hng, Y.W. Lee, S.W. Du, N.N. Thadhani, Kinetic study of thermal and impact-initiated reactions in Al–Fe_2O_3 nanothermite, Combust. Flame 157 (2010) 2241–2249.